An Investigation of Small Worldness in Pancreatic Islets

REU Site: Interdisciplinary Program in High Performance Computing

Elise Falgout[1], Destiny Frett[2], Lorenzo Neil[3], Ryan Schumm[4],
Graduate Assistant: Janita Patwardhan[5], Faculty Mentor: Brad Peercy[5], and
Client: Arthur Sherman[6]

[1]Departments of Computer Science and Mathematics, Louisiana State University,
[2]Departments of Computer Science and Mathematics, Elon University
[3]Department of Computer Science and Electrical Engineering, UMBC,
[4]Departments of Physics and Mathematics, Marquette University,
[5]Department of Mathematics and Statistics, UMBC,
[6]Laboratory of Biological Modeling, NIDDK

Technical Report HPCF–2017–14, hpcf.umbc.edu > Publications

Abstract

Diabetes occurs when the body's blood sugar levels are in a state of sustained elevation. The pancreatic beta cells, organized in the islets of Langerhans, secrete a hormone called insulin that is responsible for maintaining blood glucose at appropriate levels. Oscillations in insulin levels, which are thought to require synchronization in insulin secretion, are necessary for proper regulation of glucose. A loss of this periodic behavior has been observed in type 2 diabetic patients. We used the Single Slow Channel Model to compute the calcium and electrical dynamics during insulin secretion of a single beta cell. To replicate an islet, we coupled the cell cluster according to a hexagonal-close-packed lattice. The existence of small worldness in the islet and its effect on islet performance was investigated by using methods from graph theory. To quantify the performance, we sampled and chose a synchronization index from previously used indexes that reflects to what degree the calcium oscillations are in phase. The effect small worldness has on synchronization is indicative of the existence of hub cells, which have a larger influence on the rhythm of the islet. By destroying hub cells, we noticed that the synchronization of the islet decreased, which affects the overall performance of the islet. Understanding the role of hub cells will give us further insight on synchronization of insulin secretion between pancreatic beta cells.

Key words. diabetes, beta cells, pancreas, insulin

1 Introduction

In 2015, an estimated 30.3 million people (9.4% of the U.S. population) had diabetes and 79,535 death certificates declared diabetes to be the underlying cause of mortality, making it the seventh leading cause of death in the United States [6]. Diabetes is caused by chronically elevated glucose levels due to the improper secretion of the hormone insulin. The cells

responsible for secreting insulin are beta cells, which are located inside cell clusters in the pancreas called the Islets of Langerhans. These beta cells react to an elevated amount of glucose in the blood plasma by secreting insulin which then spurs tissues to absorb glucose from the bloodstream. Due to their key role in diabetes, beta cells have become a primary focus in diabetes research.

Recent research suggests that some beta cells hold a more pertinent role on the islets synchronization than other beta cells [7]. The existence of these hub cells is consistent with islets acting as small world networks. This idea that hub cells strongly influence the synchrony (and therefore the correct secretion of insulin) of the islet is what motivated us to investigate more thoroughly the effect that silencing some of these hub cells would have on the islets overall function.

2 Background Information

2.1 Biology

The pancreas, a major organ which influences glucose metabolism, contains clusters of beta cells called islets of Langerhans. These islets secrete the hormone insulin which encourages tissues to uptake glucose from the blood. As shown in Figure 2.1, signaling begins when glucose enters the beta cells via active transport across the cellular membrane. Glycolysis then converts glucose into pyruvate. The mitochondria further metabolize the pyruvate, increasing the ATP/ADP ratio. ATP-gated potassium channels respond to the ratio change by closing, which depolarizes the cell. This change in membrane potential allows the voltage gated calcium channels to open, resulting in an influx of calcium. The endoplasmic reticulum then releases its stored calcium, sufficiently increasing the concentration such that vesicles exocytose insulin into the blood stream. The increased blood insulin levels decrease circulating glucose, which reopens the ATP-gated potassium channels allowing the cell to repolarize and reset the cell. Normally, insulin is secreted in a pulsatile fashion, therefore oscillations in blood insulin levels are observed. Loss of this oscillatory behavior has been seen in diabetic patients [1]. The electrical synchronization among beta cells has been correlated with the pulsatility of insulin.

2.2 Single Slow Channel Model

The Single Slow Channel Model gives the electrical and calcium dynamics of an individual cell [8]. The change in time of the membrane potential is given by

$$-C_M \frac{dV}{dt} = I_{Ca}(V) + I_{K_{ATP}}(V) + I_K(V, n) + I_S(V, s) \tag{2.1}$$

where each term on the right is a current flowing through an ion channel and is balanced by the capacitive current on the left. By Ohm's Law, the current crossing a conductor is $I = gV$, where g is conductance. The concentration gradient is the driver of ion movement across the ion channels and is given by $V - E$, where V is the membrane potential and E

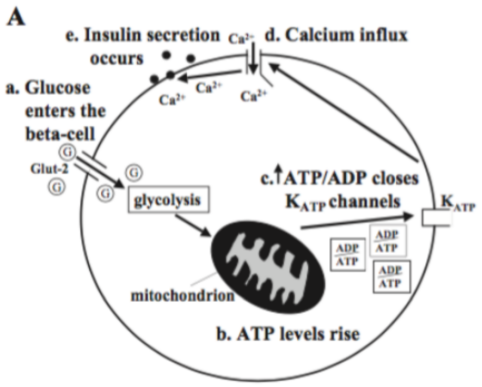

Figure 2.1: Model of beta cell insulin secretion [3]

is the Nernst potential of a given ion. Therefore, we can write the ion channel currents as $I_{ion} = g(V - E)$. The bilipid layer is modeled as a capacitor by the equation, $I_{cap} = C_m \frac{dV}{dt}$,where C_m is the capacitance of the membrane. The circuit elements are arranged in parallel, which allows us to sum the currents according to Kirchhoff's law giving equation (2.1).

The conductance for several of the ion channels is dynamic, and responds such that $g_K = \bar{g_K} n$, where n follows

$$\frac{dn}{dt} = \frac{n_\infty(V) - n}{\tau_n} \tag{2.2}$$

where n is a fraction of total voltage gated potassium channels that are open at time t. The quantity s is a gating variable related the slow inhibitory potassium current I_s and is modeled by the equation

$$\frac{ds}{dt} = \frac{s_\infty(V) - s}{\tau_s} \tag{2.3}$$

Since the calcium and ATP/ADP dependent potassium channels V gating dynamics occur so quickly, their gating variables are set to their equilibrium values m_∞ and $O_{K_{ATP}}$ respectively. The calcium concentration is modeled by

$$\frac{d[Ca^{2+}]_i}{dt} = f[-\alpha I_{Ca}(V) - k_{Ca}[Ca^{2+}]_i] \tag{2.4}$$

The first term is converts calcium current to concentration by the Faraday related constant α and the second is the rate at which calcium is pumped out of the cell. The factor f accounts for the significant slow down in calcium dynamics in the presence of buffering.

2.3 Electrical Coupling

We say two cells are coupled when there exists a gap junction such that molecules can pass between the two cells. This exchange allows the electrical state of one cell to affect that of the other. Coupling is represented mathematically by the addition of the terms $I_{ij} = g_{ij}(V_i - V_j)$

to the voltage equations, where I_{ij} is the current passing from cell j to cell i, g_{ij} is the conductance of the gap junction connecting the two cells, and V_i and V_j are the membrane potentials of cells i and j respectively. To couple all the cells in the islet, we defined the matrix M such that

$$\vec{I_c} = \begin{bmatrix} \sum_j I_{1j} \\ \sum_j I_{2j} \\ \vdots \\ \sum_j I_{Nj} \end{bmatrix} = M\vec{V} = \begin{bmatrix} \sum_{j\neq 1} g_{1j} & -g_{12} & \dots & -g_{1j} \\ -g_{21} & \sum_{j\neq 2} g_{2j} & \dots & -g_{2j} \\ \vdots & \vdots & \ddots & \vdots \\ -g_{N1} & -g_{N2} & \dots & \sum_{j\neq i} g_{Nj} \end{bmatrix} \begin{bmatrix} V_1 \\ V_2 \\ \vdots \\ V_N \end{bmatrix} \tag{2.5}$$

where the i^{th} element of $\vec{I_c}$ is the total current entering the i^{th} cell through its gap junctions, N is the number of cells in the islet, and the i^{th} element of $\vec{V}$ is the membrane potential of cell i.

3 Numerical Methods

3.1 Islet Model

The islet was modeled as a three-dimensional hexagonal-closed-packed lattice with a center maximum edge length of n and a corresponding system size given by

$$N(n) = \begin{cases} \frac{7}{2}n^3 - \frac{21}{4}n^2 + \frac{7}{2}n - 1, n \text{ is even} \\ \\ \frac{7}{2}n^3 - \frac{21}{4}n^2 + \frac{7}{2}n - \frac{3}{4}, n \text{ is odd [1].} \end{cases}$$

The lattice was assembled by stacking two-dimensional hexagonal layers that alternated between regular and irregular configurations, which can be seen in Figure 3.1. An irregular hexagon with edge length m is a regular hexagon with an edge length of $m-1$ and an extra half ring of edge length m. The locations of cells in the lattice were indexed using a Cartesian coordinate system centered on the lattice and the diameter of a cell was considered to be a single unit of distance. Two cells were considered coupled if the distance between their centers, denoted by $|\vec{x_j} - \vec{x_i}|$, is equal to one, where $\vec{x_i}$ and $\vec{x_j}$ are the position vectors of the i^{th} and j^{th} cells respectively. A cell internal to the lattice can have a maximum of twelve connections, six on the same layer, three above, three below. The square matrix, M, was used to store the coupling information such that the (i,j) entry stored the negative conductance of the gap junction connecting the i^{th} and j^{th} cells in the islet. If the entry was zero, cells i and j were not coupled. The diagonal element of the i^{th} row was given by $d_i = \sum_{j\neq i} g_{ij}$, where g_{ij} is the (i,j) gap junction conductance.

As not all cells are identical, heterogeneity was introduced in our simulations by selecting the conductance values for all ion channels from truncated normal distributions (i.e. absolute values are taken for randomly obtained negative values) with standard deviations of 5-20%

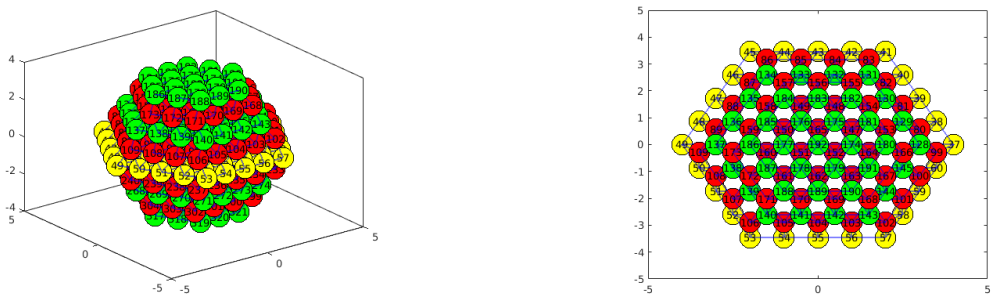

(a) (b)

Figure 3.1: (a) Side view and (b) top view of hexagonal lattice with $n = 5$

of the mean values as given in Table 3.1. Gap junction conductance values were selected from a normal distribution with a standard deviation of 50%. If a negative gap junction conductance was selected, that conductance was set to zero. In addition, 33% of the gap junction conductance values were randomly set to zero according to a binomial trial to simulate missing connections in the islet.

To simulate variations in islet coupling strength due to pharmacological or genetic modifications of gap junctions, we defined a parameter, k, selected from a normal distribution with mean $\mu \in [0,1]$ and standard deviation of 0.2. The islet coupling strength was specified by selecting the appropriate μ, which was varied for our simulations. If $k_{ij} < 0$ was selected, then we set $k_{ij} = 0$. Similarly, if $k_{ij} > 1$ was selected, then we set $k_{ij} = 1$. The (i, j) gap junction conductance was multiplied by k_{ij}, such that the coupling matrix was transformed to

$$M = \begin{bmatrix} \sum_{j\neq 1} k_{1j}g_{1j} & -k_{12}g_{12} & \dots & -k_{1j}g_{1j} \\ -k_{21}g_{21} & \sum_{j\neq 2} k_{2j}g_{2j} & \dots & -k_{2j}g_{2j} \\ \vdots & \vdots & \ddots & \vdots \\ -k_{N1}g_{N1} & -k_{N2}g_{N2} & \dots & \sum_{j\neq i} k_{Nj}g_{Nj} \end{bmatrix}$$

In order to observe how the cells establish burst synchronization and to simulate realistic islet conditions, the initial states of each cell were varied randomly by selecting values from truncated normal distributions with standard deviations equal to 20% of the mean values. Solutions to the system were computed recursively over a 500 second time-span using the ode45 MATLAB function. This algorithm is based on an explicit Runge-Kutta(4,5) formula called the Dormand-Prince pair.

Parameter/Initial Condition	Symbol	Mean value	Heterogeneity
K_{ATP} channel conductance	$g_{K(ATP)}$	100 pS	20%
Ca^{2+} channel conductance	g_{Ca}	1000 pS	5%
Voltage gated K^+ channel conductance	g_K	2700 pS	5%
Slow inhibitory K^+ channel conductance	g_s	200 pS	5%
Gap junction conductance	g_c	7.5 pS	50%
Membrane potential	V	65 mV	20%
Voltage gated K^+ channel gating variable	n	0.5	20%
Slow inhibitory K^+ channel gating variable	s	1.01	20%
Calcium concentration	$[Ca^{2+}]_i$	0.05 μM	20%

Table 3.1: Cell Heterogeneity

3.2 Small Worldness

A small world network is a mathematical graph with a high degree of local coupling and short path lengths between most nodes in the graph. Recent work has shown that small worldness may characterize the connections between cells in pancreatic islets [4]. To quantify the small worldness, we calculated the parameter $S = \frac{C_{avg}}{C_{rand}} \; / \; \frac{E_{rand}}{E_{glob}}$ of a functionally coupled beta cell network [4]. C_{avg} and E_{glob} represent the average clustering coefficient and global efficiency of the functional network respectively, while C_{rand} and E_{rand} are those values of a random network with the same number of cells and connections as the functional network. The clustering coefficient of a node measures the amount of local coupling and is defined as the number of connections between the neighbors of that node divided by the number of possible connections those neighbors can have. The global efficiency is related to the rate at which information can traverse the network. It is calculated by finding the shortest path length between each pair of nodes, and then averaging the inverse of this length. For a small world network, $C_{avg} >> C_{rand}$ and $E_{glob} \sim E_{rand}$. Hence, all graphs for which $S > 1$ are considered to be small world networks. Functional connections were created between all cells for which $P > 0.95$, where $P(c_i, c_j) = \frac{1}{N-1} \sum_t \left(\frac{c_i(t)-\langle c_j \rangle}{\sigma_i}\right)\left(\frac{c_j(t)-\langle c_j \rangle}{\sigma_j}\right)$ is the Pearson correlation coefficient computed for the calcium traces of a cell pair with $\langle \cdot \rangle$ specifying the mean of that trace [4]. The average clustering coefficients and global efficiencies of the functional and random networks were calculated using the Brain Connectivity Toolbox in MATLAB.

In biological networks, the distribution of cell connections tends to be disproportionate leading to a degree distribution that follows a power law function [7]. After the construction of the functional graph, the degree of each cell was computed and the resulting degree distribution was fit to a power law function. The cells that possessed the majority of the connections (i.e. the cells occupying the 60-100% connectivity range) were defined as network hubs.

3.3 Synchronization Index

Four indexes were used to quantify the degree of synchronization among the cells. For the first index taken from Pedersen's work, the Pearson correlation coefficient was calculated

for the calcium trace averaged over the cells and that of each individual cell [4]. A cell was considered synchronized to the islet if $P > 0.85$. The synchronization index was given by $I = \frac{L}{N}$, where L is the number of synchronized cells and N is the cell number.

The second synchronization index, taken from work done by a previous REU group, calculated the Pearson correlation coefficient for each pair of cells using the interpolated calcium traces of the cells [2]. Each coefficient was stored in a matrix such that the (i, j) entry was the correlation coefficient for the i^{th} and j^{th} cell. The average value of each row in the matrix was then calculated, and the synchronization index was defined as the minimum of these averages.

Two indexes came from Nittala's work [1]. Both utilized phase synchronization analysis which is less sensitive to variation in oscillation amplitudes than techniques that use correlation coefficients. To calculate the indexes, the instantaneous phase of the j^{th} cell was defined as $\varphi_j(t)$ and computed from the Hilbert transformation of that cell's calcium trace. Then, the mean field phase value was calculated as $\Phi(t_k) = arg \sum \exp(i\varphi_j(t_k))$. The synchronization strength of a single beta cell with the rest of the cluster was given by $\rho_j = |\langle \exp\big(i(\varphi_j(t_k)) - \Phi(t_k)\big)\rangle|$ and the total islet synchronization was defined as $\langle \rho_j \rangle = \frac{1}{n_B} \sum_j \rho_j$. The second index from Nittala assumed that all the cells were bursting. Therefore, the synchronization strength of each pair of cells could be calculated from $\lambda_{j,k} = |\langle \exp[i(\varphi_j(t) - \varphi_k(t))]\rangle|$. The index was determined by $\lambda = \langle \lambda_{j,k} \rangle = \frac{2}{(n_B)(n_B-1)} \sum_{j,k>j}^{n_B} \lambda_{j,k}$.

3.4 Chloride Modified Single Slow Channel Model

$$-C_M \frac{dV}{dt} = \sum I_{ion} + I_c - I_{Cl}$$

Using a method called optogenetics by genetically adding a light sensitive halorhodpsin molecule to beta cells, Johnston was able to silence individual cells in order to observe the effects on synchronization [7]. To replicate these biological experiments, we added a chloride channel to our Single Slow Channel Model. Similar to other ionic currents, the chloride current is modeled using a conductance (g_{Cl}), externally controlled gating variable ($\sigma(t)$), and a driving force ($V - V_{Cl}$).

$$I_{Cl} = g_{Cl}\sigma(t)(V - V_{Cl}) \text{ where } \sigma(t) = \begin{cases} 0, \, t < 100 \text{ sec} \\ \\ 1, \, t > 100 \text{ sec} \end{cases}$$

When the chloride channel is opened at $t = 100$ seconds, denoted using $\sigma(t)$, the voltage of the cell decreases. As the calcium channels are voltage dependent, the hyperpolarization of the cell prevents the larger influx of calcium, leading to the cell being silenced. We used this channel to silence individual cells, such as hub cells, and study its effect on small worldness of the entire islet.

4 Results

4.1 Replicating Previous Results

The Single Slow Channel Model was implemented in MATLAB to simulate the dynamics of an isolated single cell. To replicate bursting behavior of a cell as observed in Sherman's work, the conductance of K_{ATP} channels was set to zero and a constant was added to the differential equation controlling the slow channel gating variable s at $t = 40$ seconds, which can be seen in Figure 4.1 [8].

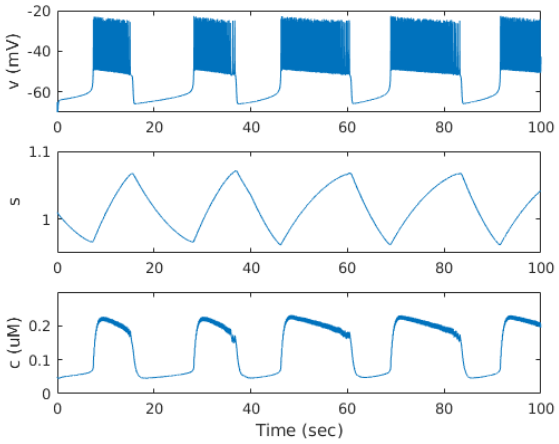

Figure 4.1: Voltage, s, and calcium time courses for isolated beta cells using the Single Slow Channel Model. At $t = 40$ sec, a constant $R = 0.5$ was added to the right-hand side of the $\frac{ds}{dt}$ equation.

To understand cell coupling, a two-cell system was simulated. The cells were coupled with the addition of a single flux term to both cells' voltage equations. Simulations were replicated from DeVries' work, one of which is shown in Figure 4.2 [5].
Initially, the voltage dynamics of the cells differed due to the varied initial conditions. Instantaneously, the cells nearly synchronize into an in-phase spiking pattern. At approximately $t = 7$, the spiking frequency increases leading to the cells bursting.

4.2 Multi-Cell Cluster Simulations

Using the hexagonal lattice, we simulated a system with 153 coupled cells ($n = 4$) with homogeneous parameters. Similar to the two cell coupled system, all cells rapidly established synchronization and bursted in phase. Since calcium can be measured experimentally, calcium traces were utilized to analyze dynamics. The beta cell lattice was visualized to observe how a calcium wave propagated through the system. The system is shown in a quiet (Figure 4.3a) and elevated (Figure 4.3b) state. The intensity of the red coloring is proportional to the calcium concentration in a cell.

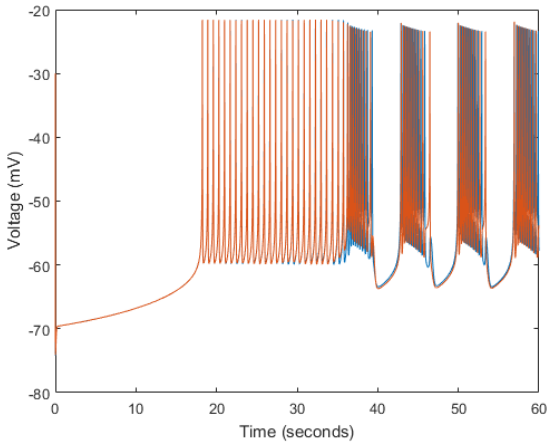

Figure 4.2: Spiking and bursting behavior between two coupled cells

(a) (b)

Figure 4.3: Hexagonal lattice with homogeneous parameters in (a) a quiet state and (b) an elevated state.

A similar system was simulated using heterogeneous instead of homogeneous parameters. Due to the differing cell parameters, some of the cells calcium concentrations were elevated before others as seen in Figure 4.4a. However, within a few seconds all cells reached a high level of calcium as seen in Figure 4.4b.

(a) (b)

Figure 4.4: Hexagonal lattice with heterogeneous parameters in (a) a quiet state and (b) an elevated state.

4.3 Synchronization

The four synchronization indexes were tested using six different coupling strengths with two tests per strength. The results are shown in Table 4.1.

μ value	Test #	Pederson	Nittala 1	Nittala 2	Previous REU
0.0	1	0.0000	0.1436	0.2013	0.0396
	2	0.0000	0.1463	0.2043	0.0281
0.2	1	0.0000	0.2212	0.1881	0.0515
	2	0.0000	0.2023	0.1875	0.0593
0.4	1	0.3282	0.8146	0.1631	0.2252
	2	0.4396	0.8139	0.1639	0.1421
0.6	1	0.6563	0.8939	0.1726	0.3952
	2	0.6656	0.9104	0.1839	0.0156
0.8	1	0.7647	0.9310	0.1922	0.0858
	2	0.7090	0.9327	0.2130	0.4966
1.0	1	0.9226	0.9530	0.2140	0.5972
	2	0.8731	0.9485	0.2279	0.5610

Table 4.1: Synchronization measurements made for six different coupling strengths using four different metrics.

The Pedersen index showed the greatest sensitivity for moderate to high coupling strengths. Nittala 1 showed better sensitivity to the low coupling strengths but saturated quickly after $\mu = 0.4$. Nittala 2 captured little variation amongst all coupling strengths. The Previous REU Synchronization Index yielded inconsistent measurements for the two tests at $\mu = 0.6$ and $\mu = 0.8$. The Pedersen index was selected to quantify synchronization for all future simulations.

Calcium and voltage time courses for three different synchronization values are shown in Figures 4.5-4.7. The cell bursting activity displayed in the graphs was recorded over a time span of 500 seconds and the different colors indicate a different cell's time course. Ten cells were selected a random from a 323-cell system and the synchronization values were obtained from the Pedersen index.

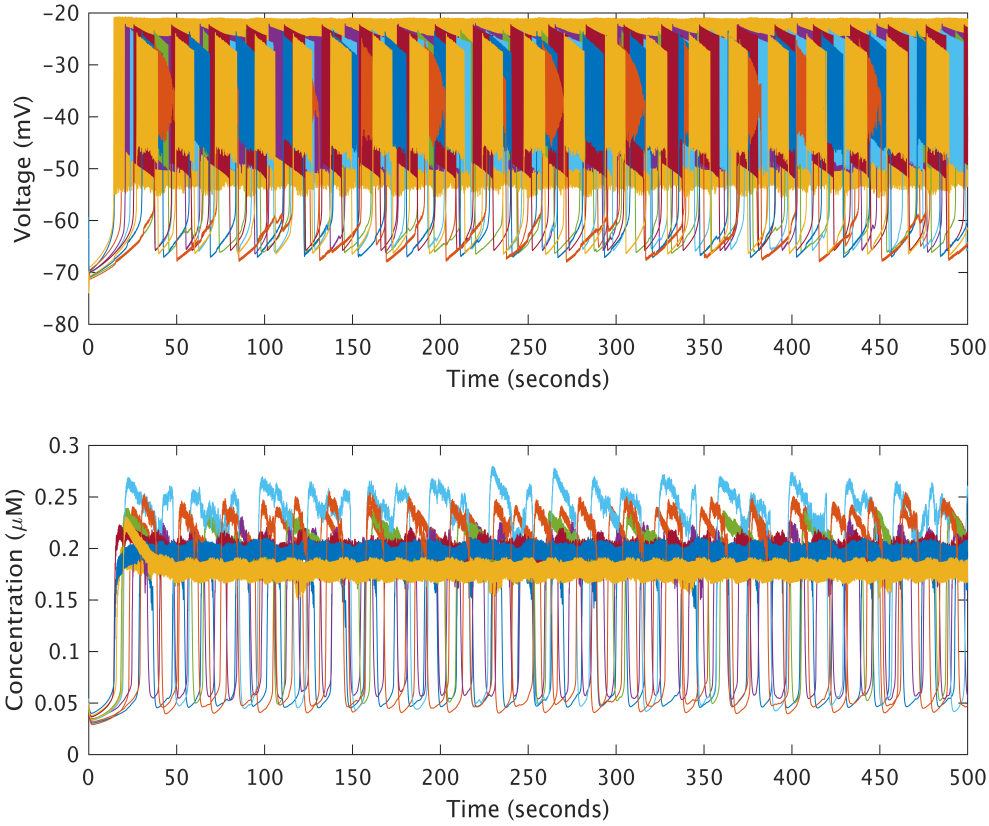

Figure 4.5: Voltage and calcium traces of 323 cells with $\mu = 0$ and synchronization index of 0

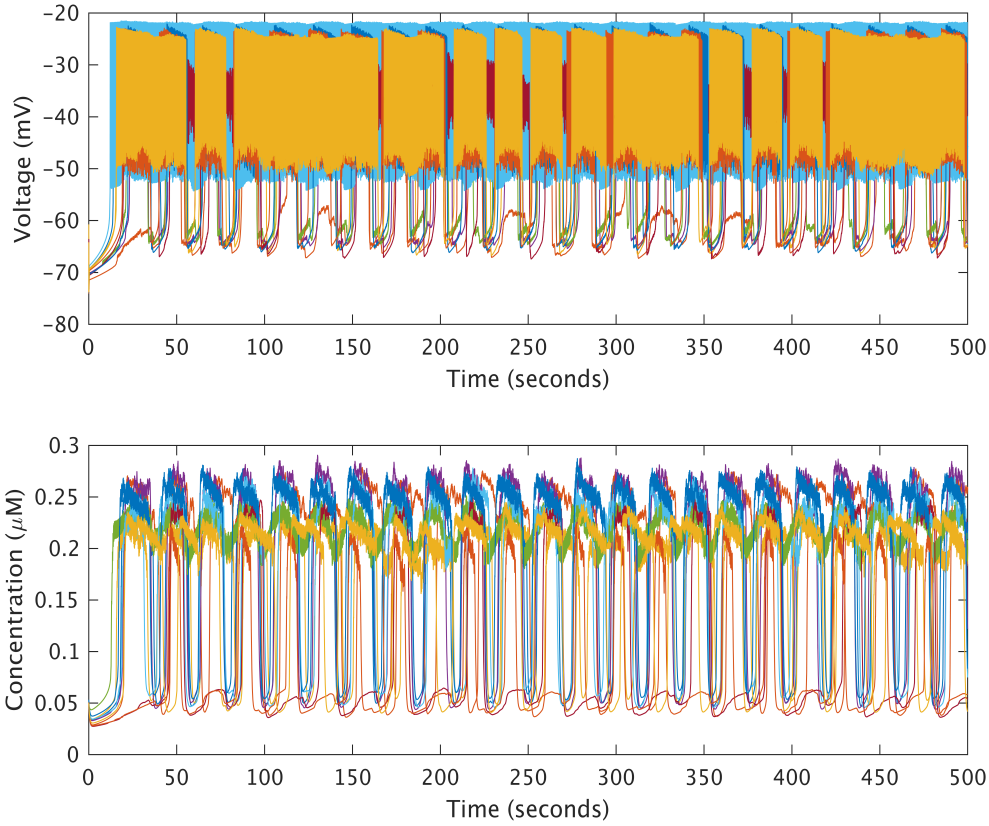

Figure 4.6: Voltage and calcium traces of 323 cells with $\mu = 0.3$ and synchronization index of 0.3331

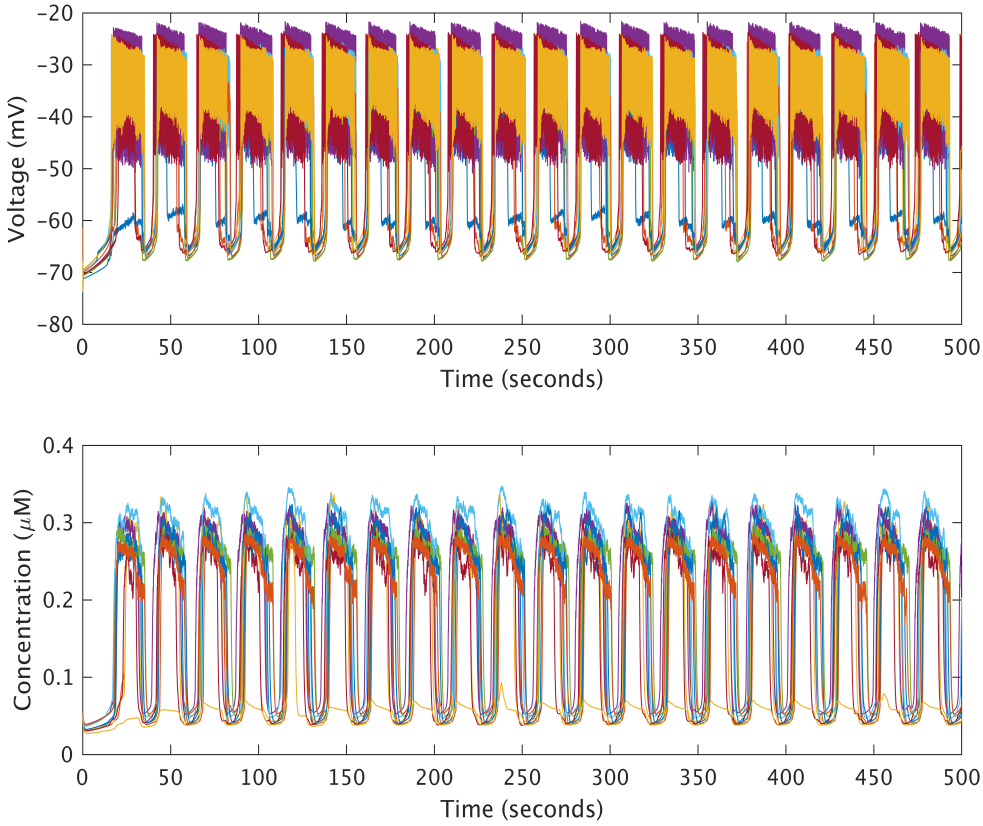

Figure 4.7: Voltage and calcium traces of 323 cells with $\mu = 0.6$ and synchronization index of 0.8773.

4.4 Small Worldness

Ten simulations were performed at each coupling strength ranging from zero to one. A 1483-cell system was used and the clustering coefficient and global efficiency were calculated for each of the ten simulations per coupling strength. The mean values are plotted in Figure 4.8a and 4.8b, respectively. Also, random networks with equal degree and edge number as the associated functional network were generated for each simulation and the mean values of the clustering coefficients and global efficiencies were obtained. The small worldness parameter was calculated for each coupling strength using the mean clustering coefficient and global efficiency (Figure 4.8c. In addition, the distribution of functional connections was calculated and a power law function was fitted to the distribution for each of the ten simulations. The mean R^2 value for the fitted curves are given in Figure 4.8d as a function of small worldness values.

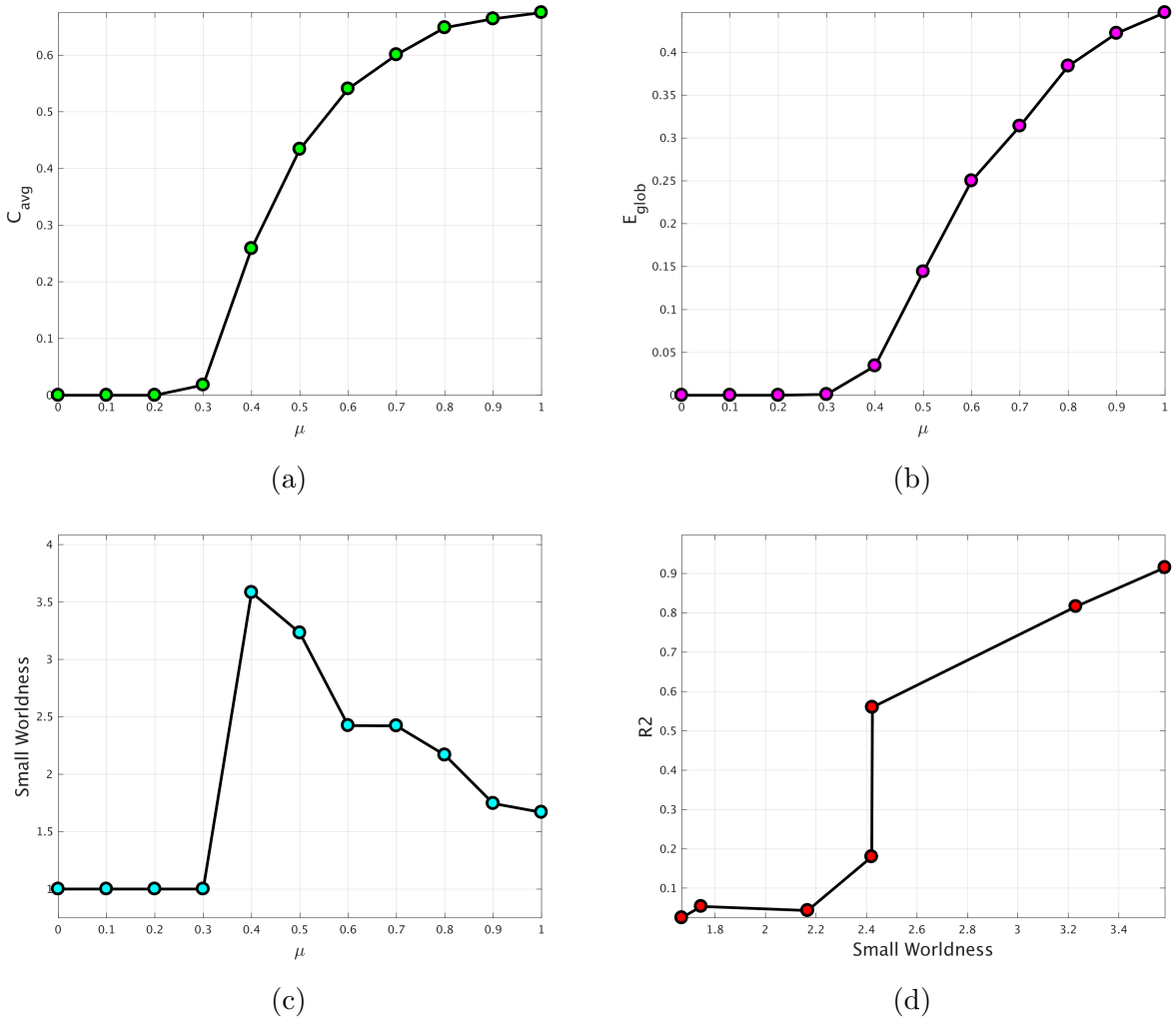

Figure 4.8: (a) Clustering Coefficient, (b) Global Efficiency, (c) Small Worldness and Coupling, (d) R^2 values for a power law function fits 1483 system

Because the number of cell pairs for which the calcium traces were correlated increased with the coupling strength, both the clustering coefficient and global efficiency increased with the coupling strength. The rate at which the normalized clustering coefficient (C_{avg}/C_r)) increased was greater than that of the normalized global efficiency, showing little to no change from $\mu = 0$ to about $\mu = 0.3$. There was a spike in small worldness between $\mu = 0.3$ to $\mu = 0.4$, then a rapid decline as the normalized global efficiency exceeded the normalized clustering coefficient due to the high number of functional connections created for high coupling strengths. The quality of the power law fit increased with the small worldness, indicating that the functional connections were distributed more disproportionately for small world networks.

4.5 Hub Cell Identification and Silencing

The functional network constructed from a previously simulated 323 cell system with a coupling strength of 0.6 is shown in Figure 4.9a

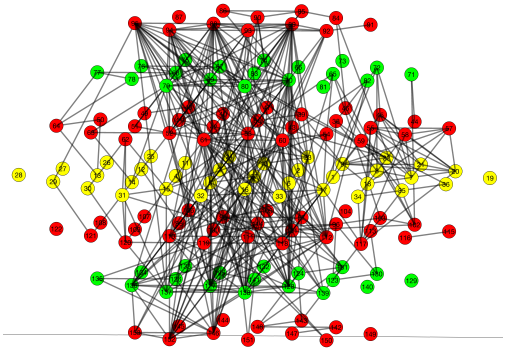

(a)

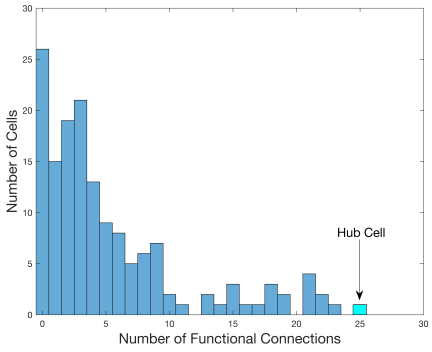

(b)

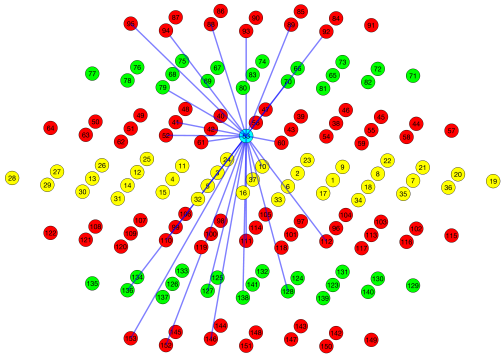

(c)

Figure 4.9: Hub cell identification in 323 network with $\mu = 0.6$. (a) Functionally coupled small world network, (b) distribution of functional connections, (c) hub cell functional connections,

and the distribution of functional connections for this system is given in Figure 4.9b. The functional network for the cell with the highest number of functional connections as labeled in Figure 4.9b is shown in Figure 4.9c. Hub cells were loosely defined as the cells with the highest numbers of functional connections.

4.6 Knockout of Few Hub Cells has Biphasic Effect on Small Worldness and Decreases Synchrony

Cells with the highest number of functional connections were then silenced and the system re-simulated. The same procedure was performed on a system with 1483 cells and a coupling strength of 0.4. The synchronization of the system after the removal hub cells is shown in Figure 4.10. As more hub cells are killed within the islet, synchronization decreases, which affects the network's overall performance.

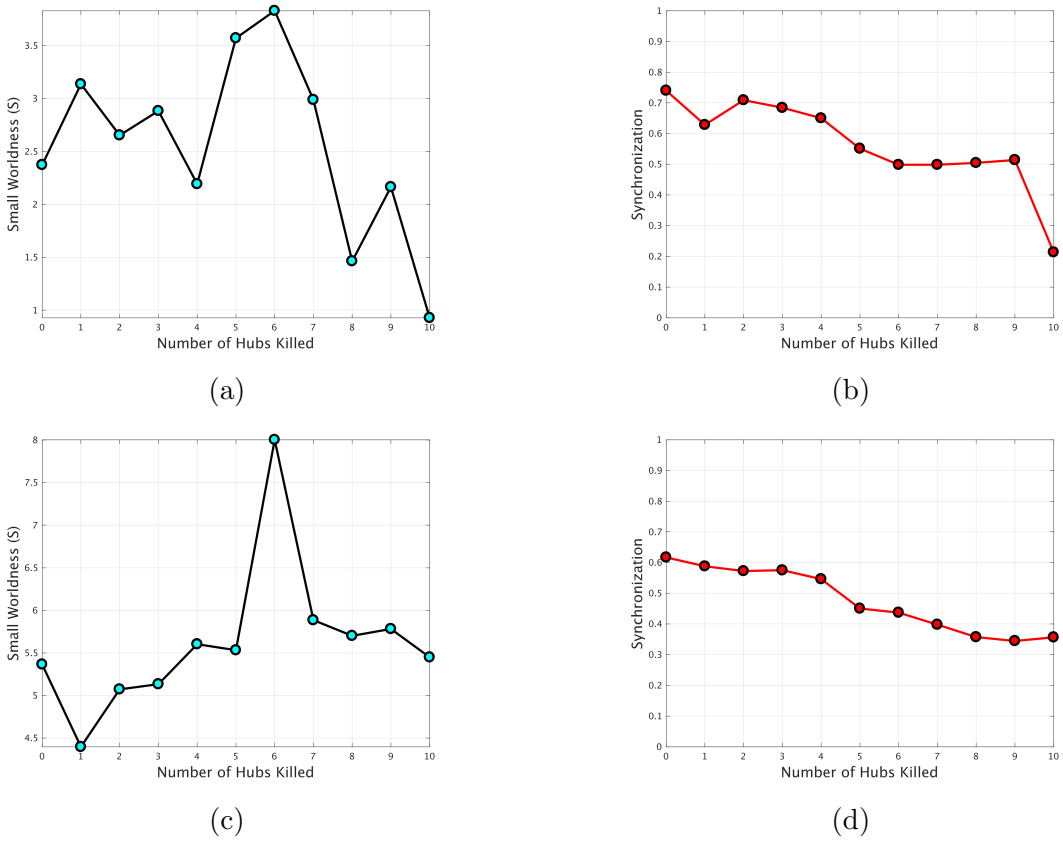

Figure 4.10: (a) Small worldness and (b) synchronization of a 323 cell system ($\mu = 0.6$) after hub cell silencing, (c) small worldness and (d) synchronization of a 1483 cell system ($\mu = 0.4$) after hub cell silencing

5 Conclusions

We have shown that networks consisting of pancreatic beta cells can be constructed with small world properties through heterogeneous nearest neighbor coupling. We saw that moderate coupling strengths generated networks with the greatest small worldness. Such coupling strengths allowed for a large number of functional connections to be formed while maintaining a disproportionate distribution of connections as shown in Figure 4.8(d). A power law connection distribution seems to be necessary to allow a select few cells in the network to act as hubs which results in high small worldness.

We saw that electrical silencing of these hubs has a destructive effect on synchronization of the islet but a biphasic effect on small worldness. Small worldness increased significantly after six hubs were silenced in both the 323 and 1483 cell islets as shown in Figure 4.10. This is likely due to a more disproportionate distribution of the remaining functional connections. But as more hubs were silenced, synchronization became too low to allow any one cell to significantly influence the islet.

In the model, as in the experiment, the β cells are still electrically coupled even under the application of light and activation of the optogenetically triggered halorhodopsin Cl channels. Remaining electrically connected means that the optogenetically activated cells will act as a bit of a current sink. This had the effect of reordering which cells were the most connected cells in the islet once a more connected cell was optogenetically removed. However, when we removed subsequent hub cells we referred to the original list of hub cells. It is likely we if were to remove hub cells after reordering, we would find an even more dramatic fall off in synchronization and possibly a more rapid rise and decent in small worldness.

It apears that small worldness likely increases the vulnerability of an islet to damage. In Figure 4.10, we saw that destruction of only 0.7% of the cells in a 1483 cell islet reduced the synchronization from about 0.63 to 0.35, and destruction of only 3% of the cells in a 323 cell islet reduced synchronization from 0.76 to 0.2. It was also observed that for a given coupling strength, a 1483 cell islet had more small worldness than a 323 cell islet. This implies that larger islets are more vulnerable than smaller islets due to the greater control that hub cells have on synchronization in the larger network. Studies have shown that obese individuals tend to have more cells per islet than healthy individuals. Hence, if beta cell communication is mediated by a highly small world network in the larger islets of obese individuals, hub destruction may lead to loss of islet synchronization and the acquisition of diabetes.

Acknowledgments

These results were obtained as part of the REU Site: Interdisciplinary Program in High Performance Computing (hpcreu.umbc.edu) in the Department of Mathematics and Statistics at the University of Maryland, Baltimore County (UMBC) in Summer 2017. This program

is funded by the National Science Foundation (NSF), the National Security Agency (NSA), and the Department of Defense (DOD), with additional support from UMBC, the Department of Mathematics and Statistics, the Center for Interdisciplinary Research and Consulting (CIRC), and the UMBC High Performance Computing Facility (HPCF). HPCF is supported by the U.S. National Science Foundation through the MRI program (grant nos. CNS–0821258 and CNS–1228778) and the SCREMS program (grant no. DMS–0821311), with additional substantial support from UMBC. Co-author Lorenzo Neil was supported, in part, by the UMBC National Security Agency (NSA) Scholars Program through a contract with the NSA. Graduate assistant Janita Patwardhan was supported by UMBC.

References

[1] Xujing Wang Aparna Nittala, Sourmitra Ghosh. Investigating the role of islet cytoarchitecture in its oscillation using a new beta-cell cluster model. *PLoS ONE*, pages 1–17, 2007.

[2] Mary Aronne, Samantha Clapp, Soohwan Jung, Abigail Kramer, William Wang, Janita Patwardhan, Bradford E Peercy, and Arthur Sherman. The interaction of calcium and metabolic oscillations in pancreatic β-cells. *Spora: A Journal of Biomathematics*, 3(1):1, 2017.

[3] Richard Bertram, Arthur Sherman, and Leslie S Satin. Metabolic and electrical oscillations: partners in controlling pulsatile insulin secretion. *American Journal of Physiology-Endocrinology And Metabolism*, 293(4):E890–E900, 2007.

[4] Giacomo Cappon and Morten Gram Pedersen. Heterogeneity and nearest-neighbor coupling can explain small-worldness and wave properties in pancreatic islets. *Chaos: An Interdisciplinary Journal of Nonlinear Science*, 26(5):053103, 2016.

[5] Gerda De Vries and Arthur Sherman. From spikers to bursters via coupling: help from heterogeneity. *Bulletin of mathematical biology*, 63(2):371–391, 2001.

[6] Centers for Disease Control and Prevention. 2017 national diabetes statistics report, 2017.

[7] Natalie R Johnston, Ryan K Mitchell, Elizabeth Haythorne, Maria Paiva Pessoa, Francesca Semplici, Jorge Ferrer, Lorenzo Piemonti, Piero Marchetti, Marco Bugliani, Domenico Bosco, et al. Beta cell hubs dictate pancreatic islet responses to glucose. *Cell metabolism*, 24(3):389–401, 2016.

[8] Arthur Sherman. Contributions of modeling to understanding stimulus-secretion coupling in pancreatic beta-cells. *Modeling in Physiology Invited Review*, pages 362–372, 1996.